2010 Fourth Pacific-Rim Symposium on Image and Video Technology

High-quality Non-blind Image Deconvolution

Jong-Ho Lee and Yo-Sung Ho
Gwangju Institute of Science and Technology (GIST)
261 Cheomdan-gwagiro, Buk-gu, Gwangju 500-712, Korea
e-mail: {jongho, hoyo}@gist.ac.kr

***Abstract*—The most annoying artifacts in image deconvolution are ringing and amplified noise. These artifacts can be reduced significantly by regularization using the Maximum a Posteriori (MAP) method that exploits not only the likelihood but also the image prior in image deconvolution. Although ringing and noise can be reduced significantly with strong regularization, image details are also reduced, so the deconvolved image is neither sharp nor clear. In this paper, we propose a non-blind image deconvolution method with adaptive regularization that can reduce ringing and noise more noticeable in a smooth region and preserve image details in a textured region. For adaptive regularization, after we make a quick estimate of the reference image that can indicate the strength of regularization, we perform regularization adaptively according to the local characteristics. Experimental results show that ringing and noise are suppressed significantly, while preserving image details effectively.**

Keywords-non-blind image deconvolution; maximum a posteriori; adaptive regularization

I. INTRODUCTION

Camera motion blur is one of the most common and unpleasant defects in photography. If the motion blur is shift-invariant, recovering a true latent image from a degraded image reduces to image deconvolution. The blurring process is commonly modeled as a convolution of the true latent image and a kernel with additive noise:

$$B = I \otimes K + N \ , \tag{1}$$

where B is the degraded image, I is the true latent image, K is the kernel, and N is additive noise.

If both the kernel and the latent image are unknown, the problem is called blind deconvolution. On the other hand, if the only latent image is unknown, the problem is called non-blind deconvolution. In this paper, our target is non-blind deconvolution. In many cases, the kernel can be estimated effectively. Fergus *et al*. estimated the kernel from a single image using variational Bayesian approach [1]. Ben-Ezra and Nayer estimated the kernel using a secondary sensor [2]. Yuan *et al*. estimated the kernel from a blurred image and a noisy image [3].

However, non-blind deconvolution is still an ill-posed problem although the kernel is known, so it gives rise to artifacts in the deconvolved image. The main artifacts are ringing and noise amplification. Ringing is the ripple-like artifact that appears around strong edges in the deconvolved image as shown in Fig. 1 (b). Kernel is often band-limited, so its frequency response shows near-zero values at the high frequency. Therefore, the direct inverse of the kernel with the blurred image causes large signal amplification at the high frequency components. This is represented as ringing near the edges and amplified noise. Especially, kernel estimation errors accelerate the ringing artifacts and give unpleasant deconvolved results. Although many effective blind deconvolution algorithms are proposed, estimating the kernel is a still tough problem. If the blurred image has saturated pixels or the latent image does not contain sharp edges, the blind deconvolution algorithms often fail to find correct kernels. Thus, the kernel estimation errors which cause severe ringing artifacts and noise amplification are inevitable.

(a) (b)

Figure 1: Ringing artifacts in image deconvolution. (a) Deconvolution result. (b) A magnified patch.

It is useful to include the image prior into deconvolution to overcome these artifacts. The prior helps to reduce ringing and noise while recovering the latent image. However, this regularization technique works well only for small-size kernels and small kernel estimation errors. If the kernel size or kernel estimation errors are large, the artifacts are also increased, and strong regularization is needed to reduce these artifacts. The strong regularization reduces artifacts significantly, but it also reduces image details.

We propose a non-blind image deconvolution method with adaptive regularization that can reduce ringing and noise effectively in a locally smooth region and preserve image details in a textured region so that the high-quality deconvolved image can be resulted in. First, we estimate a reference image that indicates right edge information of the latent image, and adaptive regularization is performed referring to this estimated reference image. In the reference image estimation and adaptive regularization, we use adaptive bilateral filtering and adaptive shock filtering to enhance the result.

978-0-7695-4285-0/10 $26.00 © 2010 IEEE
DOI 10.1109/PSIVT.2010.54

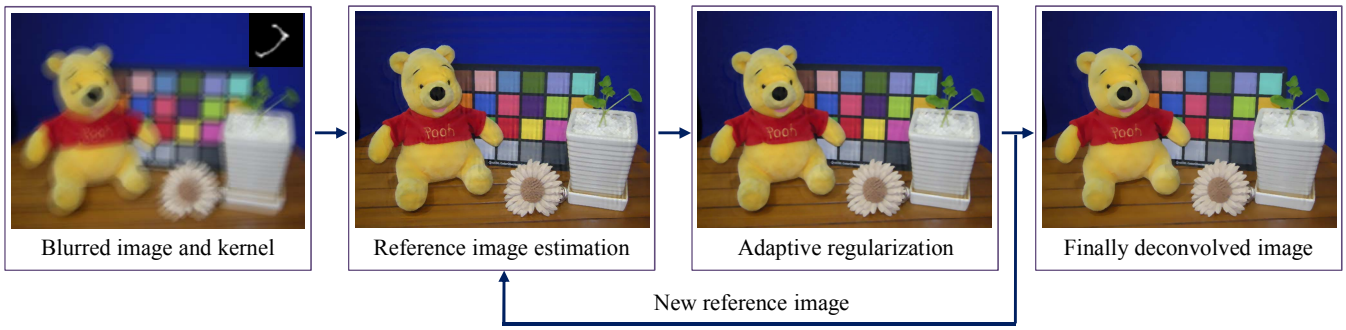

Figure 2: Overview of our algorithm.

II. Related Work

In non-blind deconvolution, the kernel is assumed to be known or estimated in other ways. Thus, the remaining task is to estimate true latent image. Wiener filtering [6] and Richardson-Lucy method [7] are traditional and popular non-blind deconvolution methods. They were proposed decades ago, but are still widely used for image restoration because they are simple, fast, and gives good results in case of the relative small-size blur. However, these methods are weak to image noise and kernel estimation error, so they suffer from ringing artifacts. Donatelli *et al*. use a PDE-based model to recover a latent image with reduced ringing by incorporating an anti-reflective boundary condition and a re-blurring step [13]. Regularization techniques using image prior are also proposed to avoid these artifacts. Dey *et al*. proposed total variation regularization with Laplacian prior [8]. Levein *et al*. used a sparse prior that shows excellent results without ringing artifacts [9]. However, all these non-blind deconvolution methods are effective when the kernel size is small and the kernel has no error. Otherwise, the deconvolved image contains severe ringing artifacts and amplified noise.

In blind deconvolution, the problem is more challenging because the kernel as well as the latent image is unknown. Additional input is used to facilitate the problem in some methods. Yuan *et al* use a pair of images, a blurred image and a noisy image, to estimate the kernel and deblur the blurred image [3]. Ben-Ezra and Nayar attach a low-resolution video camera to a high-resolution still camera to help in recording the kernel [1]. Recently, the kernel was estimated from a single image. Fergus *et al*. used a variational Bayesian method with natural image statistics to estimate the kernel [1]. Jia used an alpha matte that describes transparency changes caused by a motion blur for kernel estimation [10]. Shan *et al*. proposed the deblurring method using a MAP to estimate the kernel and the latent image from a single image [4].

However, all the above methods fail to preserve image details and reduce artifacts at the same time in the deconvolution because it is difficult to locate proper edge information in the blurred image.

III. Overview

The main idea of our algorithm is to change the strength of regularization according to the local characteristics of the latent image. For this adaptive regularization, right edge information is needed, but unfortunately, it is not available in the blurred image. Thus, we make the reference image temporally which indicates the textured region and the smooth region much better than the blurred image. This reference image is estimated fast in the frequency domain using FFTs (Fast Fourier transforms).

On the other hand, Adaptive regularization is performed in the spatial domain using the estimated reference image. The strength of regularization on each pixel of the blurred image is controlled by the reference image. The deconvolved image with adaptive regularization is set to the second reference image, and adaptive regularization is performed again. Since the new reference image shows the edge information better than the first reference image, it gives better deconvolved result.

In the reference image estimation and adaptive regularization, we also use adaptive bilateral filtering and adaptive shock filtering to enhance the performance of the algorithm. Fig. 2 represents the overall procedure of our algorithm.

IV. Reference Image Estimation

The reference image is to locate the smooth region and the textured region correctly. However, it is difficult to distinguish between two regions perfectly at one try. Thus, the reference image is estimated by iteration. First, a temporal reference image is estimated by combination of fast image deconvolution using hyper-Laplacian priors [5] and the model of the spatially random distribution of image noise [4]. This combination enables the reference image to be estimated fast with enhanced image details.

Fast image deconvolution using hyper-Laplacian uses an alternating minimization scheme where the non-convex part of the problem is solved in one phase, followed by a quadratic phase which can be efficiently solved in the frequency domain using Fast Fourier Transforms (FFTs). Thus, the latent image I^* can be estimated very fast with the following equations.

$$I^* = \arg\min_I \sum_{i=1}^{N} \left(\frac{\lambda}{2}(I \otimes K - B)_i^2 + \sum_{j=1}^{2} |(I \otimes f_j)_i|^{\alpha}\right)$$
$$= \arg\min_I \sum_{i=1}^{N} \left(\frac{\lambda}{2}(I \otimes K - B)_i^2 + \frac{\beta}{2}(\|(I \otimes f_1)_i - w_i^1\|_2^2 \right. \quad (2)$$
$$\left. + \|(I \otimes f_2)_i - w_i^2\|_2^2) + |w_i^1|^{\alpha} + |w_i^2|^{\alpha}\right),$$

where I^* is the estimated latent image, i is the pixel index, $f_1=[1\ -1]$, $f_2=[1\ -1]^T$, β is a weight that will be varied during the optimization, w_i^1 and w_i^2 are auxiliary variables that allow the term $(I \otimes f_j)_i$ to be moved outside the $|.|^{\alpha}$.

The model of the spatially random distribution of image noise states that not only image noise but also its higher-order partial derivatives follow Gaussian distributions with different standard deviations as follows [4].

$$p(B \mid I) = \prod_{\partial^* \in \Theta} \prod_i N(\partial^* B_i \mid \partial^*(I \otimes K)_i, \sigma_q^2), \quad (3)$$

where ∂^* denotes the operator of any partial derivative with $k(\partial^*)=q$ representing its order. $\partial^* N=\partial^*(B-I \otimes K)$ follows a Gaussian distributions with standard deviation $\sigma_q=\sqrt{2^q}\,\sigma_0$, where σ_0 denotes the standard deviation of N. $\Theta = \{\partial_0, \partial_x, \partial_y, \partial_{xx}, \partial_{xy}, \partial_{yy}\}$ represents a set of partial derivatives.

The reference image I^* is generated by combining (2) and (3) as follows.

$$I^* = \arg\min_I \sum_{i=1}^{N} \left(\frac{\lambda}{2}\left(\sum_{\partial^* \in \Theta} \tau_{k(\partial^*)} \|(\partial^* I \otimes K - \partial^* B)_i\|^2\right)\right.$$
$$+ \frac{\beta}{2}(\|(I \otimes f_1)_i - w_i^1\|^2 + \|(I \otimes f_2)_i - w_i^2\|^2) \quad (4)$$
$$\left. + |w_i^1|^{\alpha} + |w_i^2|^{\alpha}\right),$$

where $\tau_{k(\ *)}=1$, 0.5, and 0.25 when $k(\ \ *)=0$, 1, and 2 respectively. To solve (4), $w=\{w_1, w_2\}$ values are calculated first with the method introduced in [5], and the reference image I^* is estimated with (4) given a fixed value of w. $\lambda=8 \times 10^3$ and $\alpha=2/3$ are used to estimate I^*. Equation (4) can be solved using 2D FFT very fast assuming circular boundary conditions. We applied the algorithm proposed in [12] to reduce the boundary artifacts caused by FFT.

Although the I^* estimated by (4) has reduced ringing artifacts and noise due to regularization, and shows edge information much better than the blurred image, it still has small ringing artifacts and noise, and its edges are slightly blurred. To solve these problems, we apply an adaptive bilateral filter and an adaptive shock filter to I^*.

The adaptive bilateral filter is to reduce small ringing artifacts and noise in I^* which are not removed completely even with regularization. To reduce ringing artifacts and noise while preserving edges, strong filtering is applied to the smooth region and weak filtering is applied to the textured region. Since the region without any edges in the blurred image is also the smooth region in the latent image, the pixel p satisfying the following equation is judged to be in the smooth region Ω.

$$p \in \Omega \ \text{if}\ Eg(p) < T_b$$
$$Eg(p) = \left(\sum_{h \in W_x} h + \sum_{v \in W_y} v\right) / N_{total}, \quad (5)$$

where $Eg(p)$ is the edge strength at the pixel location p on the blurred image, $W_x=W \otimes [1\ -1]$, $W_y=W \otimes [1\ -1]^T$, W is the 3×3 window whose center is located on p, and N_{total} is the total number of pixels of W. $T_b=2 \times 10^{-5}$ is used for the experiment. The adaptive bilateral filtering on I^* is performed with the following equation.

$$F(I^*(p)) = \frac{1}{Z}\sum_{p' \in N} G_d(p-p', \sigma_d)\, G_r(I^*(p) - I^*(p'), \sigma_r) I^*(p') \quad (6)$$
$$\text{with} \begin{cases} \sigma_d = 5\sigma_0 \text{ and } R_N = 5R_0 & \text{if } p \in \Omega \\ \sigma_d = \sigma_0 \text{ and } R_N = R_0 & \text{elsewhere} \end{cases},$$

where G_d and G_r are Gaussian functions with standard deviations σ_d and σ_r respectively. N is a neighboring window, R_N is a radius of N, and Z is a normalization term. $R_0=1$, $\sigma_0=4$, and $\sigma_r=0.05$ are used for the filtering.

After adaptive bilateral filtering, the ringing artifacts and noise in I^* are significantly reduced, but edges in I^* are blurred because of regularization and adaptive bilateral filtering. We use an adaptive shock filter to recover these slightly blurred edges selectively. The shock filter is an effective filter to recover sharp edges from slightly blurred step signals [12], and the adaptive shock filter performs the recovering process adaptively according to the local characteristics. The evolution equation of the adaptive shock filter is as follows.

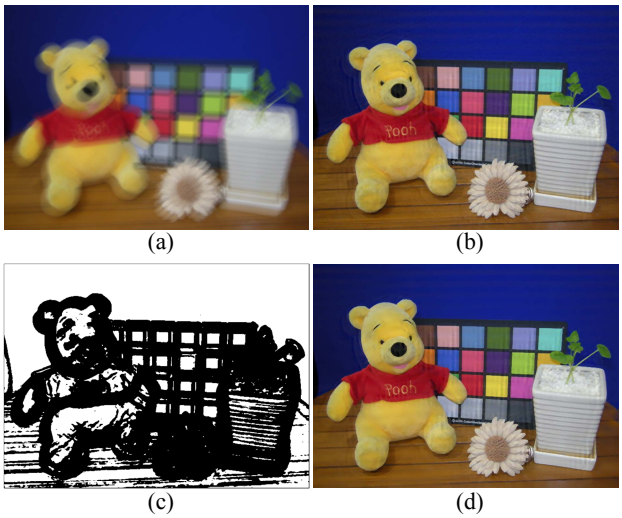

Figure 3: Reference image estimation. (a) Blurred image. (b) Result of (4). (c) Smooth region Ω in white. (d) Result after simple filtering operations on (b).

$$I_{t+1} = I_t - M(p)sign(\nabla^2 I_t) \| \nabla I_t \| dt$$
$$with \;\; M(p) = \begin{cases} 0 & if \;\; p \in \Omega \\ 1 & elsewhere \end{cases}, \quad (7)$$

where I_t is an image at time t, and ∇^2 and ∇ are the Laplacian and gradient respectively. dt is the time step for a single evolution. The interim result images described in section 4 are represented in Fig. 3.

V. ADAPTIVE REGULARIZATION

The reference image estimated in section 4 provides edge information much better than the blurred image, but the fine scale detail layer is suppressed and ringing and noise are still noticeable. We perform adaptive regularization using the reference image to obtain the deconvolved result with enhanced image details and suppressed ringing and noise simultaneously.

According to Bayes framework, the posteriori for the latent image is written as:

$$p(I \mid B) \propto p(B \mid I) p(I), \quad (8)$$

where $p(B|I)$ denotes the likelihood of the blurred image given the latent image, and $p(I)$ represents the image prior. The MAP solution of I can be obtained by minimizing the following energy:

$$I^* = \underset{I}{argmin}\, E(I), \quad (9)$$

where

$$E(I) = -log\; p(I \mid B) = -log\; p(B \mid I) - log\; p(I) \quad (10)$$

The likelihood is based on noise, $N = B - I \otimes K$. For this likelihood, we adopt the model of the spatially random distribution of image noise [4] that is described in (3). We also adopt the sparse distribution as the image prior [9]:

$$p(I) = exp(-\alpha(|I \otimes f_1|^{0.8} + |I \otimes f_2|^{0.8})), \quad (11)$$

where f_1=[1 -1] and f_2=[1 -1]^T.

By taking the likelihood and the prior into (10), we get

$$E(I) = \sum_{\partial^* \in \Theta} \tau_{k(\partial^*)} \| (\partial^* I \otimes K - \partial^* B)_i \|^2 + \eta(|I \otimes f_1|^{0.8} + |I \otimes f_2|^{0.8}), \quad (12)$$

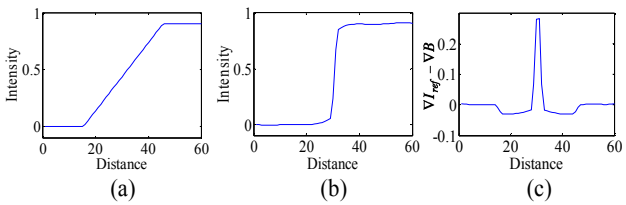

(a) (b) (c)

Figure 4: Local characteristics. (a) Step signal of the blurred image. (b) Step signal of the reference image. (c) Difference between the derivative of (b) and the derivative of (a).

where $\eta = 2\sigma_0^2 \alpha$. η is the regularization weighting factor that controls the strength of regularization. For adaptive regularization, η should have an effect on each pixel with different intensity according to the local characteristics.

Fig. 4 shows the step signals of the blurred image and the reference image and the difference between the derivatives of step signals of the reference image and the blurred image. When the blurred image is deconvolved, the step signal of the blurred image with a gentle slope becomes steeper. That is, the derivative of the step signal of the reference image is larger than that of the step signal of the blurred image. This causes the big difference between the derivatives of the step signals of the reference image and the blurred image at the real edges, and this fact can be used for good criteria for detecting real edges to perform adaptive regularization.

Based on this criteria, $E(I)$ in (12) is modified as follows.

$$E(I) = \sum_{\partial^* \in \Theta} \tau_{k(\partial^*)} \| (\partial^* I \otimes K - \partial^* B)_i \|^2 + \eta H(\nabla I_{ref} - \nabla B)(|I \otimes f_1|^{0.8} + |I \otimes f_2|^{0.8}) \quad (13)$$
$$with\; H(x) = \begin{cases} 0 & if\; x > T_a \\ 1 & elsewhere \end{cases}$$

If the $(\nabla I_{ref} - \nabla B)(p)$ on pixel p is larger than T_a, the pixel p is considered to be in the textured region, so no regularization is performed on that pixel. Otherwise, the pixel p is considered to be in the smooth region, and strong regularization is performed on that pixel. $T_a = 2 \times 10^{-5}$ was used for our experiments. Fig. 5 (a) shows $H(\nabla I_{ref} - \nabla B)$ map. The smooth region is represented in white and the textured region in black. To solve (13), iterative re-weighted least squares (IRLS) algorithm is used. IRLS poses the optimization as a sequence of least squares problems, while each least square problem re-weighted by solution at the previous step [9].

The result image after adaptive regularization suppresses the ringing artifacts and noise in the smooth region while preserving image details in the textured region. For better result, this image is set as the new reference image since it shows better edge information than the first reference image. Adaptive regularization is performed again based on the new reference image.

(a) (b)

Figure 5: Adaptive regularization. (a) $H(\nabla I_{ref} - \nabla B)$ map. (b) Finally deconvolved image.

After final adaptive regularization, the smooth region is detected on the finally adaptive-regularized result image. Based on this detected smooth region, adaptive bilateral filtering is used to remove small ringing and noise remained in the adaptively regularized image, and adaptive shock filtering based on the detected smooth region is used to enhance the fine scale detail layer.

Fig. 5 (b) shows the results of adaptive regularization. When compared to the first reference image in Fig. 3 (b), the finally deconvolved image shows that the ringing artifacts and noise are reduced significantly without losing sharpness of edges.

VI. Experimental Results

We applied our algorithm to the synthesized image and the real blurred image. The synthesized image is generated by convolving the artificial kernel and the original image. For the synthesized image, both objective quality and subjective quality are checked. For the real blurred image, only subjective quality is checked. The kernels of all images are estimated by Fergus *et al*'s single image blind deconvolution method [2]. We compare our algorithm with four other non-blind image deconvolution methods, the standard Richardson-Lucy (RL) method [7], Total variation (TV) regularization [8], Levin *et al*'s method [9] and Shan et *al*'s non-blind deconvolution method [4]. For fare comparison, we tune the regularization parameters of all algorithms to produce the best results.

Fig. 6 shows the comparison of the subjective quality in case of the synthesized "Beer" image. The estimated kernel size is 37 x 37, and the size of blurred image is 664 x 489. The RL method preserves edges very well but produces the most noticeable ringing and noise. The TV regularization reduces ringing and noise significantly, but image details are also reduced. The Levin *et al*'s algorithm and the Shan *et al*'s algorithm reduce ringing effectively without large image details loss, but they show limitations in case of large kernel errors since the same regularization weighting factors are applied to all pixels of the image. However, our algorithm shows the good result with reduced ringing and noise in smooth region effectively, while preserving image edges well by adjusting the regularization weighting factor according to the local characteristics.

For the synthesized image, the objective quality also can be compared since we already know the original image. Table 1 shows the comparison of objective quality. We used (14) for the comparison metric. We calculated and compared the SNR for R, G, B channels and luminance component of the deconvolved images. Our algorithm shows the best performance compared to other non-blind image deconvolution methods.

$$SNR(dB) = 10\log_{10}\left(\frac{\| I-\mu(I)\|^2}{\| I-I^*\|^2}\right), \qquad (14)$$

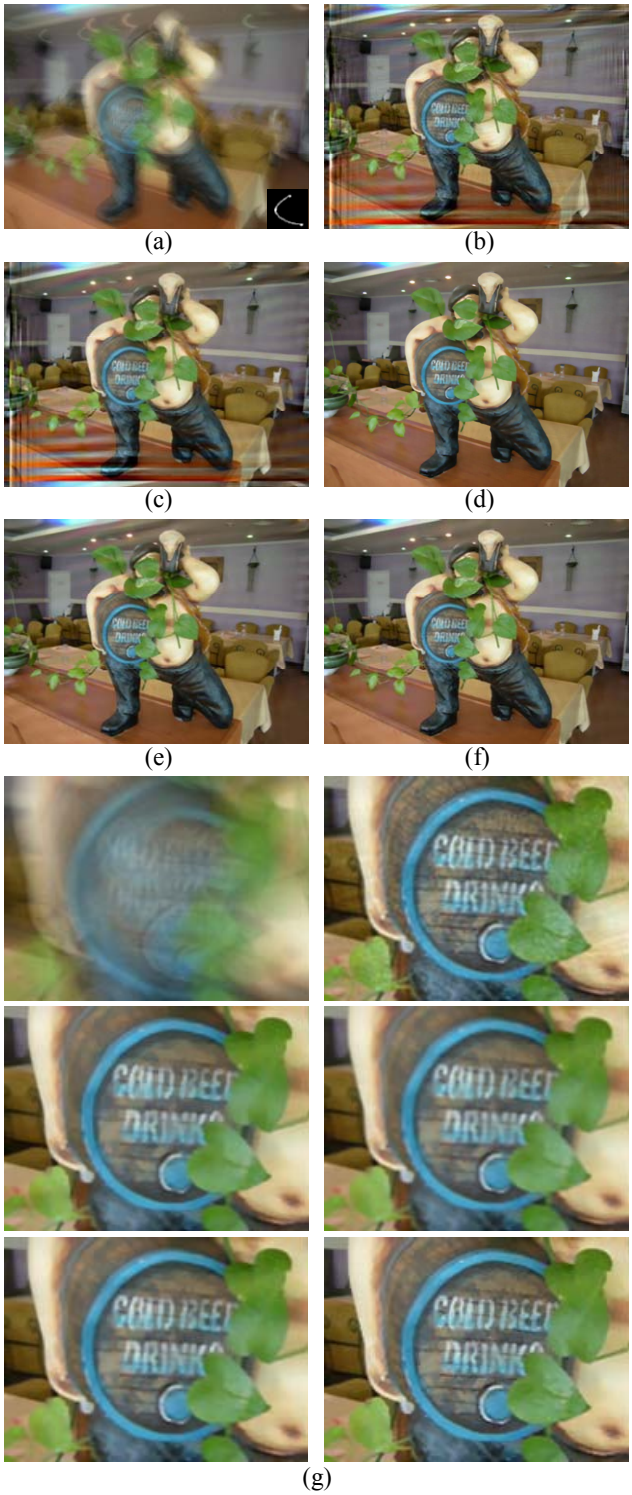

Figure 6: Beer. (a) Blurred image and estimated kernel. (b) Richardson-Lucy method. (c) TV regularization. (d) Levin *et al*. (e) Shan *et al*. (f) Our method. (g) Close-up views of (a)-(f).

where I is the original image, $\mu(I)$ is the mean of I, and I^* is the deconvolved image.

Table 1: Comparison of *SNR*s for the "Beer" image

Method	*SNR_R*	*SNR_G*	*SNR_B*	*SNR_Y*
RL	8.6460	6.4081	5.8152	7.7587
TV	7.9823	5.4414	3.9164	6.7483
Levin *et al*'s	15.6266	15.4895	15.1118	15.5924
Shan *et al*'s	14.7365	15.1967	14.9486	14.9606
Ours	16.0644	15.7858	15.3756	16.0915

Figure 7: Statue. (a) Blurred image and estimated kernel. (b) TV regularization. (c) Levin *et al*'s method. (d) Our method. (e) Close-up views of (a)-(d).

Figure 7 shows the results for the real blurred image. Our result shows the smallest ringing in the background and the most improved image details when compared with other methods.

VII. Conclusion

The most notorious artifacts at image deconvolution are ringing artifacts and noise amplification. This problem is solved using the image prior that represents global statistics of the image. However, strong regularization for reducing artifacts at image deconvolution does not preserve image details. In this paper, we have presented the adaptive regularization method with help of the reference image that separates the smooth region from the textured region. The experimental results show that our approach suppresses ringing artifacts effectively, while preserving image details.

Acknowledgment

This research was supported by the MKE(The Ministry of Knowledge Economy), Korea, under the ITRC(Information Technology Research Center) support program supervised by the NIPA(National IT Industry Promotion Agency) (NIPA-2010-(C1090-1011-0003)).

References

[1] Fergus, R., Singh, B., Hertzmann, A., Roweis, S.T., Freeman, W.T. Removing Camera Shake from a Single Photograph. *ACM Trans. on Graph*. (*SIGGRAPH*), 25: 787-794, 2006.

[2] Ben-Ezra, M.R., Nayar, S.K. Motion Deblurring using Hybrid Imaging. *Proceedings of Computer Vision and Pattern Recognition*, 1:657-664, 2003.

[3] Yuan, L., Sun, J., Quan, L., Shum, H.Y. Image Deblurring with Blurred/Noisy Image Pairs. *ACM Trans. on Graph*. (*SIGGRAPH*), 26:1-10, 2007.

[4] Shan, Q., Jia, J.Y., Agarwala, A. High-quality Motion Deblurring from a Single Image. *ACM Trans. on Graph.* (*SIGGRAPH*), 27, 2008.

[5] Krishnan, D., Fergus, R. Fast Image Deconvolution using Hyper-Laplacian Priors. *Advances in Neural Information Processing Systems*, 22:1-9, 2009.

[6] Wiener, N. Extrapolation, Interpolation, and Smoothing of Stationary Time Series, *MIT Press*, 1964.

[7] Lucy, L. An Iterative Technique for the Rectification of Observed Distributions, *Astronomical Journal*, 79: 745-754, 1974.

[8] Dey, N., Blanc-Fraud, L., Zimmer, C., Kam, Z., Roux, P., Olivo-Marin, J. Zerubia, J. Richardson-Lucy Algorithm with Total Variation Regularization for 3D Confocal Microscope Deconvolution. *Microscopy Research Technique*, 69: 260-266, 2006.

[9] Levin, A., Fergus, R. Durand, F., Freeman, W.T. Image and Depth from a Conventional Camera with a Coded Aperture. *ACM Trans. on Graph.* (*SIGGRAPH*), 26: 70-77, 2007.

[10] Jia, J. Single Image Motion Deblurring using Transparency. *Proceedings of Computer Vision and Pattern Recognition*, 1-8, 2007.

[11] Osher, S., Rudin, L.I. Feature-oriented Image Enhancement using Shock Filters. *SIAM Journal on Numerical Analysis*, 27: 919-940, 1990.

[12] Lee, J. H., Ho, Y. S. Non-blind Image Deconvolution with Adaptive Regularization. *Lecture Note in Computer Science*, To be published, 2010.

[13] Donatelli, M., Estatico, C., Martinelli, A., Serra-Capizzano, S. Improved Image Deblurring with Anti-reflective Boundary Conditions and Re-blurring. *Inverse Problems*, 22 : 2035-2053, 2006.